SCIENTIFIC REPORTS

OPEN

SUBJECT AREAS:
THEORY AND COMPUTATION
CONDENSED-MATTER PHYSICS

Received
7 July 2014

Accepted
29 September 2014

Published
10 November 2014

Correspondence and requests for materials should be addressed to T.C. (cuitian@jlu.edu.cn)

Pressure-induced metallization of dense $(H_2S)_2H_2$ with high-T_c superconductivity

Defang Duan[1,2], Yunxian Liu[1], Fubo Tian[1], Da Li[1], Xiaoli Huang[1], Zhonglong Zhao[1], Hongyu Yu[1], Bingbing Liu[1], Wenjing Tian[2] & Tian Cui[1]

[1]State Key Laboratory of Superhard Materials, College of physics, Jilin University, Changchun, 130012, P. R. China, [2]State Key Laboratory of Supramolecular Structure and Materials, Jilin University, Changchun, 130012, P. R. China.

The high pressure structures, metallization, and superconductivity of recently synthesized H_2-containing compounds $(H_2S)_2H_2$ are elucidated by *ab initio* calculations. The ordered crystal structure with *P*1 symmetry is determined, supported by the good agreement between theoretical and experimental X-ray diffraction data, equation of states, and Raman spectra. The *Cccm* structure is favorable with partial hydrogen bond symmetrization above 37 GPa. Upon further compression, H_2 molecules disappear and two intriguing metallic structures with *R*3m and *Im*-3*m* symmetries are reconstructive above 111 and 180 GPa, respectively. The predicted metallization pressure is 111 GPa, which is approximately one-third of the currently suggested metallization pressure of bulk molecular hydrogen. Application of the Allen-Dynes-modified McMillan equation for the *Im*-3*m* structure yields high T_c values of 191 K to 204 K at 200 GPa, which is among the highest values reported for H_2-rich van der Waals compounds and MH_3 type hydride thus far.

Closed shell systems (e.g., H_2O, H_2S, CH_4, SiH_4, GeH_4, NH_3BH_3, Ar, Kr, and Xe) can absorb additional H_2 molecules under high pressure conditions, forming a series of new H_2-containing stoichiometric compounds, such as $H_2O(H_2)$[1], $(H_2S)_2H_2$[2], $CH_4(H_2)_4$[3], $SiH_4(H_2)_2$[4,5], $GeH_4(H_2)_2$[6], $NH_3BH_3(H_2)_x$[7,8], $Ar(H_2)_2$[9], $Kr(H_2)_4$[10], and $Xe(H_2)_8$[11]. Given their high amount of hydrogen, these compounds are potential energy storage materials and high-temperature superconductors. For example, $CH_4(H_2)_4$ with 33.4 wt% high hydrogen content is a potentially high hydrogen storage material[12]. Metallic hydrogen is one of the most important physical problems in high-pressure research, which is believed to be a room-temperature superconductor[13,14]. However, the metallization of hydrogen is still under debate in laboratories[15,16]. Hydrogen-rich compounds, such as GaH_3[17], GeH_3[18], Si_2H_6[19,20], SiH_4[21–24], GeH_4[25], KH_6[26], CaH_6[27], $SiH_4(H_2)_2$[28], and $GeH_4(H_2)_2$[29] are extensively explored as alternatives because their metallization can occur at relatively lower pressures through chemical pre-compressions, which present high temperature superconductivity. H_2-containing compounds $SiH_4(H_2)_2$ and $GeH_4(H_2)_2$ have been predicted to have high T_c values of 98 K to 107 K at 250 GPa and 76 K to 90 K at 250 GPa (with the Coulomb parameter $\mu^* = 0.1$–0.13), respectively[28,29]. For the MH_3 (M = Ga, Ge, Si) type hydride, T_c is estimated theoretically to be 76 K to 86 K ($\mu^* = 0.1-0.13$) at 160 GPa[17], 140 K ($\mu^* = 0.13$) at 180 GPa[18], and 139 K to 153 K ($\mu^* = 0.1-0.13$) at 275 GPa[19], respectively. Theoretical predictions also revealed that the T_c of sodalite-like CaH_6 at 150 GPa reached 220 K to 235 K ($\mu^* = 0.1-0.13$)[27]. Considering that H_2 is the most abundant substance in the universe, the behavior of H_2-containing compounds over a broad P–T range is important for planetary sciences.

Recently, Strobel *et al.* reported that mixing hydrogen sulfide (H_2S) and hydrogen (H_2) can form a stoichiometric compound $(H_2S)_2H_2$ near 3.5 GPa, which is characteristic of a rotationally disordered structure[2]. X-ray diffraction (XRD) results have indicated that this structure belongs to the tetragonal space group *I4/mcm*. The experimental Raman data indicated that an ordering process occurred with structural transformation above 17 GPa. A candidate structure with space group *I*222 was proposed by a*b initio* density functional theory (DFT) calculations through structural optimizations. However, obtaining the most stable structure only by structural relaxation is difficult because of potential energy barrier. Another unexpected structure can possibly become stable instead.

We have taken a new route in this study using the recently fast-developed evolutionary algorithm Universal Structure Predictor: Evolutionary Xtallography (USPEX)[30–32] to explore the high-pressure ordered crystal structures of $(H_2S)_2H_2$. We found that a triclinic (*P*1) structure is energetically favorable. Motivated by the metallization and potential high-temperature superconductivity in $(H_2S)_2H_2$, higher pressure structures have been

extensively explored. Our calculations reveal a metallization pressure of 111 GPa and a high T_c of 200 K at 200 GPa. The lower metallization pressure is within the reach of current diamond–anvil techniques, which will inevitably stimulate extensive experiments.

Results

Variable-cell structure prediction simulations with 1 to 4, 6, and 8 H_3S formula units per cell (f.u./cell) at pressures between 20 and 300 GPa were performed. A group of new structures was uncovered under high pressure—triclinic *P*1 (8 f.u./cell), orthorhombic *Cccm* (16 f.u./cell), trigonal *R*3*m* (3 f.u./cell), and cubic *Im*-3*m* (2 f.u./cell) as shown in Fig. 1. The lattice parameters of these structures at different pressures are also listed in Table S1 of the supplementary information.

Enthalpy difference curves (relative to the *Cccm* structure) for different structures are presented in Fig. 2. *P*1 is the most stable structure below 37 GPa, which has lower energy than that of the proposed experimental *I*222 structure[2]. This *P*1 structure consists of an ordered H-bonded H_2S network and two anti-parallel hydrogen molecules occupying the interstitial sites. One molecule lies at z = 0, whereas the other lies at the z = 1/2 plane (Figs. 1a and 1b). The *Cccm* structure is energetically stable between 37 and 111 GPa. Unlike the *P*1 structure, partial hydrogen bond symmetrization is formed in the *Cccm* structure. This structure consists of 3D H_2S networks that trap two different types of hydrogen molecules in channels: one type is arranged such that the head-tail hydrogen molecule (H2–H2) alignment follows the *c*-axis, whereas the other type is characterized by parallel hydrogen molecule (H1–H1) configuration pointing to the *b*-axis (Figs. 1c and 1d). The absence of any imaginary frequency also confirms the dynamic stability of the *P*1 and *Cccm* phases (see supplementary Fig. S1).

The lattice angles $\alpha = 90.12^\circ$, $\beta = 89.85^\circ$, and $\gamma = 90.15^\circ$ is approximately equal to 90° for the *P*1 structure at 20 GPa (see supplementary Table S1), which can thus be viewed as a slightly distorted orthorhombic lattice. This condition can explain the experimental suggestion of an orthorhombic structure. We compared the XRD patterns of the *P*1 structure with that of the experimental pattern in Fig. 3a. A theoretical pattern was obtained with the same X-ray wavelength of 0.39796 Å as the experimental one. The simulated XRD patterns for the *P*1 structures agree well with those for the experiment data[2]. The calculated equation of states (EOS) for the *P*1 structure was also compared with experimental one in Fig. 3b. Good agreement between the theoretical and experimental results provides another support for the validity of the *P*1 structure. Given that hydrogen atoms are undetectable by XRD patterns, the Raman spectrum of *P*1 is presented for comparison with the experimental results (see supplementary Fig. S2). Two H_2 vibron-peaks are well reproduced, and the two low-frequency features agree qualitatively between theory and experiment. This Raman result, together with the XRD and EOS evidence, support our predicted *P*1 structure in $(H_2S)_2H_2$.

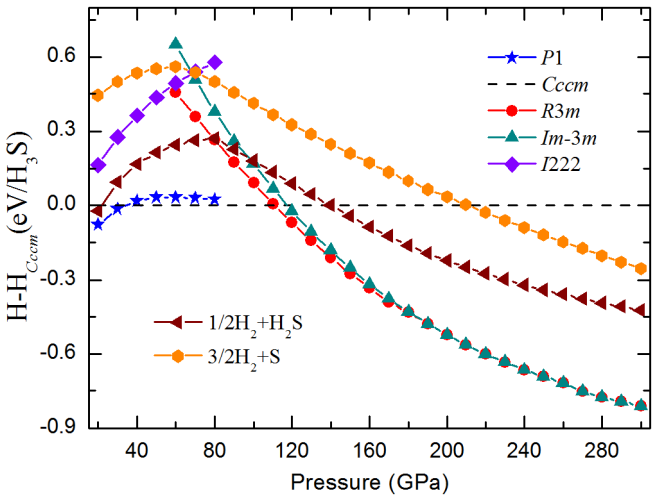

Figure 2 | Calculated enthalpies per H_3S unit as the function of pressure. Calculated enthalpy curves for various structures relative to our predicted *Cccm* structure as a function of pressure. The decomposition enthalpies into S+3/2H_2 and H_2S+1/2H_2 are also plotted.

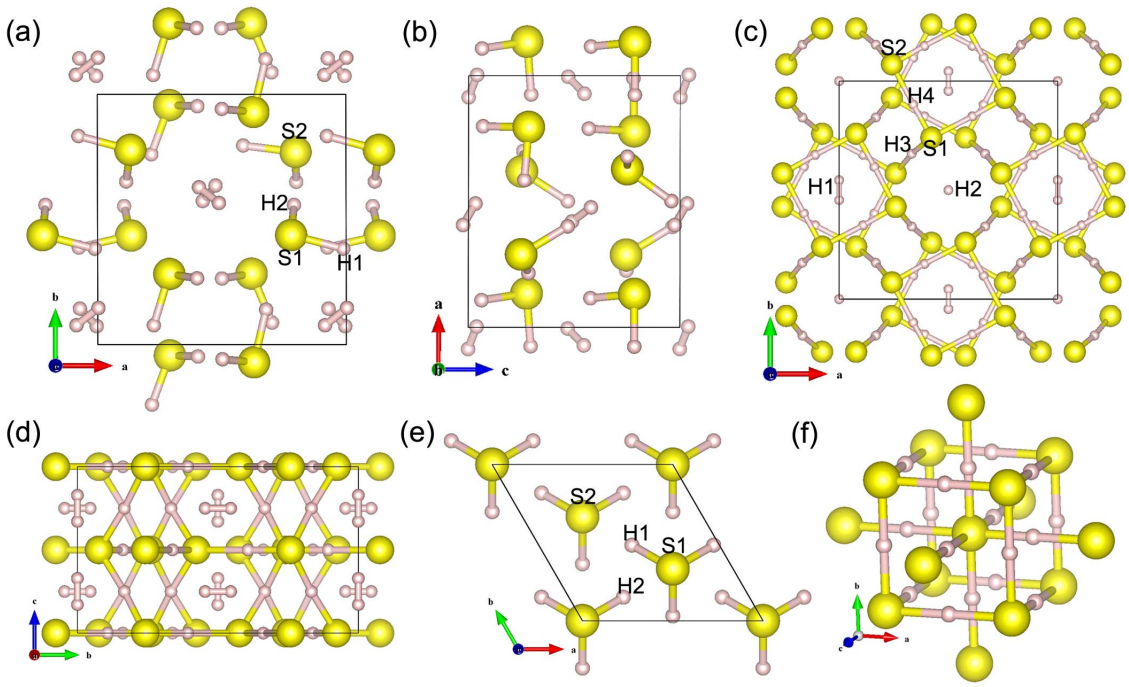

Figure 1 | High-pressure crystal structures of $(H_2S)_2H_2$. (a) *P*1 structure normal to the (001) plane, (b) *P*1 structure normal to the (010) plane, (c) *Cccm* structure normal to the (001) plane, (c) *Cccm* structure normal to the (100) plane, (e) *R*3*m*, and (f) *Im*-3*m*. Large spheres represent S and small spheres denote H atoms, respectively.

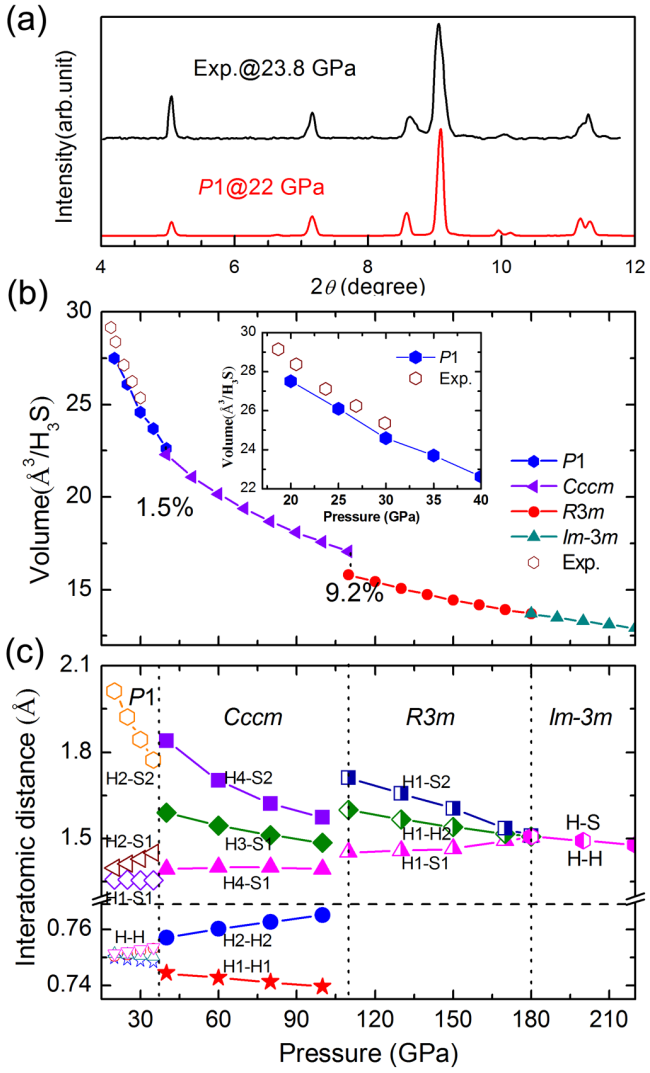

Figure 3 | Calculated XRD and EOS compared with experiment data. (a) The simulated XRD patterns and (b) calculated EOS for the *P*1 structures compared with experiment data (ref. 2). (c) Various interatomic distances of *P*1, *Cccm*, *R*3*m*, and *Im*-3*m* structures with pressure.

The *Cccm* structure transforms to a denser *R*3*m* structure above 111 GPa with a volume collapse of 9.2% on further compression (Fig. 3b). The *R*3*m* structure shows a disappearing H_2 molecule and forms a pyramidal H_3S molecular unit as depicted in Fig. 1e. A high-symmetry *Im*-3*m* structure becomes favorable above 180 GPa. This structure is characterized by two S atoms located at a simple body centered cubic lattice and H atom located symmetrically between the S atoms (Fig. 1f). The hydrogen bond symmetrization completed in the *R*3*m*→*Im*-3*m* transition is observed. The coordination number of the S atom increased from three to six with the formation of hydrogen-shared SH_6.

The decomposition enthalpies into S + H_2 and H_2S + H_2 are examined to check the phase stability of $(H_2S)_2H_2$ under pressure (Fig. 2). The structures of $P6_3m$, $C2/c$, and *Cmca* for H_2[33], $I4_1/acd$[34], and β-Po[35] for S, $P2/c$, Pc, $Pmc2_1$, P-1, and *Cmca* for H_2S[36] in their corresponding stable pressures are adopted. The most stable phases of $(H_2S)_2H_2$ have lower enthalpy than S + H_2 and H_2S + H_2 over the pressure range of 20 GPa to 300 GPa. Thus, the $(H_2S)_2H_2$ crystal remains stable against decomposition in our studied pressure range. The calculated pressure–volume data of $(H_2S)_2H_2$ is also shown in Fig. 3b. The volume collapses with 1.5% for *P*1 to *Cccm* transition and 9.2% for *Cccm* to *R*3*m* transition, suggesting a first-order phase transition character, whereas the volume change is continuous for *R*3*m* to *Im*-3*m* transition, supporting a second-order nature.

The pressure dependence of the nearest intramolecular and intermolecular bond distances are plotted in Fig. 3c to understand the molecular interactions observed in $(H_2S)_2H_2$. Four types of intramolecular H–H bond lengths are nearly equal with distances of approximately 0.75 Å and slightly longer than that 0.74 Å in solid H_2 at 20 GPa, indicating a weak interaction between H_2S and H_2. The two H–H bond lengths increased, whereas the other two decreased with increasing pressure, consistent with the observed redshift and blueshift of H–H Raman vibrons[2], respectively. The hydrogen bond (H2···S2) is also relatively weak with distance of 2.01 Å at 20 GPa. The strength of the hydrogen bond gradually increases with increasing pressure and significantly elongates one of the H2–S1 covalent bonds for a single molecule. The length of the H3–S1 bond (symmetrization hydrogen bond) is 1.59 Å, the H4–S1 covalent bond is 1.39 Å, and the H4···S2 bond is 1.84 Å in the *Cccm* structure at 40 GPa, indicating a strong hydrogen bond. The length of the strong hydrogen bond decreases, whereas the length of the H4–S1 bond slightly increases with increasing pressure. Notably, the length of the H1–H1 bond decreases to 0.744 Å, whereas the length of the H2–H2 bond increases to 0.757 Å at 110 GPa (Fig. 3d), indicating a slightly increased interaction between S and H2 under pressure. The *R*3*m* structure is reconstructive with the disappearing H_2 molecule and forms new H-S bonds at 111 GPa. Thus, a large kinetic barrier is formed for the transformation from *Cccm* to *R*3*m*. The length of the H1–S1 bond increases with increasing pressure, whereas the length of the hydrogen bond (H1···S2) decreases. Thus, the hydrogen bond symmetrized completely accompanied by the *R*3*m*→*Im*-3*m* phase transition at a pressure of 180 GPa. The nearest H–H distance at 110 GPa in the *R*3*m* structures is 1.599 Å, much longer than the H–H bond length of ~1.2 Å in CaH_6 which is characteristic of a weak covalent bond[27]. The H–H distance decreases slowly and becomes 1.433 Å at 300 GPa with increasing pressure, indicating that H and H atoms do not present any bond.

The electronic band structure and projected density of states (DOS) for all $(H_2S)_2H_2$ structures were also explored. The *P*1 structure is an insulator with an indirect band gap of 3.34 eV at 20 GPa (see supplementary Fig. S3). The bands are flat, indicating that the *P*1 structure is a typical molecular crystal. The band gap for the *Cccm* structure decreases with increasing pressure and closes at approximately 110 GPa. Given the deficiency of DFT associated with generalized gradient approximation (GGA), the calculated band gaps are likely to be underestimated. Therefore, the *Cccm* structure should be an insulator in its stable pressure range. Notably, both the *R*3*m* and *Im*-3*m* structures are good metals with a large DOS at the Fermi level, as shown in Fig. 4. The projected DOS clearly indicates strong hybridizations of S and H orbitals. Energy band structures near the Fermi level for both *R*3*m* and *Im*-3*m* are characterized as "flat band-steep band", indicating that they may be good superconductors[37]. The predicted metallization pressure of 111 GPa is significantly lower than the currently suggested pressure for the metallization of bulk molecular hydrogen[38].

The calculated phonon dispersion curves and projected phonon DOS for *R*3*m* and *Im*-3*m* structures are presented in Fig. 5. The absence of any imaginary frequency indicates their dynamical stability. The low-frequency bands come mainly from the vibrations of the S atom, whereas higher-frequency modes are mostly related to the H atoms. The electron phonon coupling (EPC) λ, logarithmic average phonon frequency ω_{log}, and the Eliashberg phonon spectral function $\alpha^2F(\omega)$[39] are investigated to explore the possible superconductivity of $(H_2S)_2H_2$. The resulting λ of *R*3*m* is 2.07 at 130 GPa, indicating a fairly strong EPC; the ω_{log} calculated from the phonon spectrum is 1125.1 K. The calculated λ of *Im*-3*m* is 2.19 at 200 GPa, whereas the ω_{log} is 1334.6 K. Using the calculated ω_{log} and commonly accepted values of the Coulomb pseudopotential μ^* (0.1–

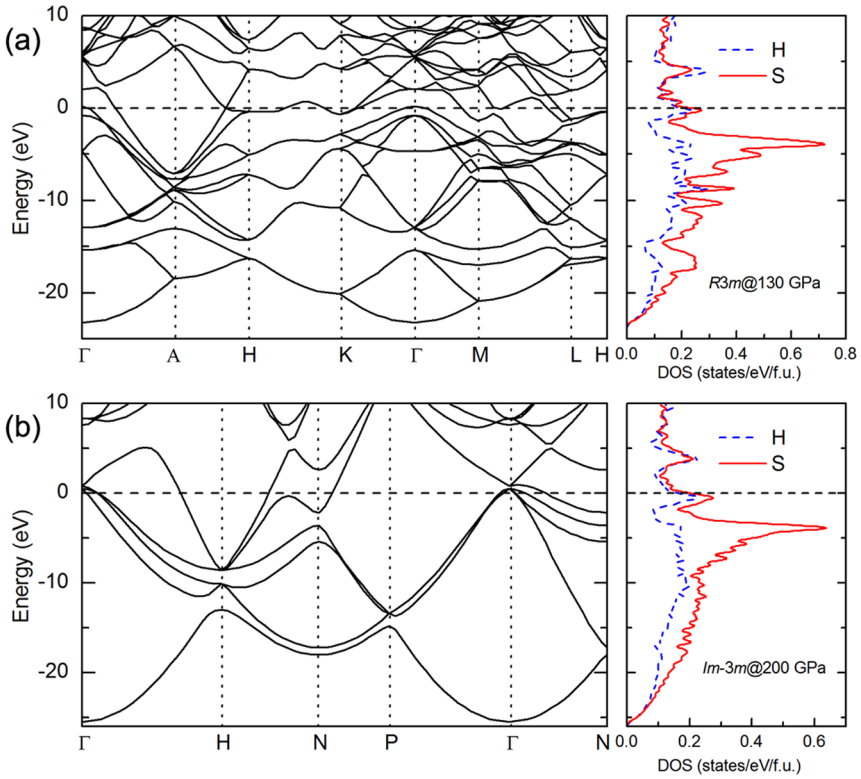

Figure 4 | Electronic band structure and density of states (DOS). Electronic band structure and atom-projected DOS for (a) *R*3*m* at 130 GPa and (b) *Im*-3*m* at 200 GPa along the selected high symmetry lines, where the dotted lines at zero indicate the Fermi level.

0.13)[40] from the Allen-Dynes-modified McMillan equation[41], the superconducting transition temperature T_c for *R*3*m* was obtained in the range of 155 K to 166 K at 130 GPa. Similarly, the calculated T_c for the *Im*-3*m* structure at 200 GPa reaches high values of 191 K to 204 K. T_c decreases nearly linearly with pressure (184 K at 250 GPa and 179 K at 300 GPa for $\mu^* = 0.13$) at an approximate rate (dT_c/dP) of −0.12 K/GPa for the *Im*-3*m* structure.

Discussion

Motivated by the metallization and potential high-temperature superconductivity in hydrogen-rich materials of $(H_2S)_2H_2$ or H_3S, high-pressure structures at a wide pressure range of 20 GPa to 300 GPa were extensively explored. Four order structures under high pressure have been predicted: *P*1 (stable below 37 GPa), *Cccm* (stable at 37 GPa–111 GPa), *R*3*m* (stable at 111 GPa–180 GPa), and *Im*-3*m* (stable above 180 GPa). The *R*3*m* and *Im*-3*m* structures are good metals above 111 GPa. The estimated T_c of the *Im*-3*m* phase at 200 GPa is 191 K–204 K, which are among the highest values reported for H_2-rich van der Waals compounds[28,29] and MH_3 (M = Ga, Ge, Si)-type hydride[17–19] thus far. In a survey of literature, many similarities in structures, metallization, and superconductivity for the MH_3[17–19] are observed. They all have a high-symmetry cubic structure under high pressure, with high superconducting transition temperature. The lowest T_c value is 86 K for GaH_3. They are also good metals at an experimentally accessible pressure, with the highest metallization pressure at 190 GPa for Si_2H_6. Although the crystal structure-predicting methods implemented by USPEX code are efficient for global structural convergence, it is limited by the sizes of the simulation cell employed. Given that the number of energy minima on the potential-energy surface grows exponentially with increasing cell size, making an extensive structural search is impossible. Thus, we cannot rule out the possibility that the actual high-pressure phase of $(H_2S)_2H_2$ with larger unit cells may exist.

Notably, no H_2 molecules were observed in the *R*3*m* and *Im*-3*m* structures. However, H_2 molecules still exist up to 300 GPa for other H_2-containing compounds[28,29,42], such as $SiH_4(H_2)_2$, $GeH_4(H_2)_2$, and $Ar(H_2)_2$, although the intramolecular H–H bond was stretched under high pressure. We calculated the electron localization function (ELF) to understand the bonding nature in the *R*3*m* and *Im*-3*m* structure (Fig. 6). The ELF value for the S–H bonds is close to 1.0, which suggests a strong polar covalent bond. The ELF value between the nearest H–H is very low, indicating the absence of covalent bond characteristics between hydrogen atoms. This scenario is different from MH_3 (M = Ga, Ge, Si)[17–19], where the charge transfer from M to H atoms forms a strong ionic character. We propose a possible formation process of covalent bond in the *R*3*m* structure as follows: the H_2 molecules dissociated to hydrogen atoms under high pressure, and the hydrogen atoms then cooperated with sulfur atoms to form a strong polar covalent bond. This strong bond makes the H and S atoms tightly bound to form a dense H_3S structure, yielding the reduction of its volume.

The predicted high T_c for $(H_2S)_2H_2$ or H_3S in the order of ~200 K is very encouraging, which prompted us to study the underlying superconducting mechanism. The corresponding Eliashberg spectral function $\alpha^2F(\omega)$ and integrated λ as a function of the frequency for the *R*3*m* at 130 GPa and *Im*-3*m* at 200 GPa are presented in Fig. 5. S vibrations in the frequency region below 15 THz contribute approximately 33.1% in total λ for the *R*3*m* structure, whereas H vibrations above 18 THz contribute 66.9% of λ. The low-frequency S vibrations (< 18 THz) and high-frequency H vibrational mode (> 20 THz) contribute 18.4% and 82.6% to the EPC, respectively, for the *Im*-3*m* structure. This result highlights that the H atoms play a significant role in superconductivity, although the S vibrations at low frequencies are also contributors. This physical mechanism is similar to GaH_3[18] and $GeH_4(H_2)_2$[29], but different from $SiH_4(H_2)_2$[28] where the strong interactions between H_2 and SiH_4 molecules vibrations dominate the superconductivity.

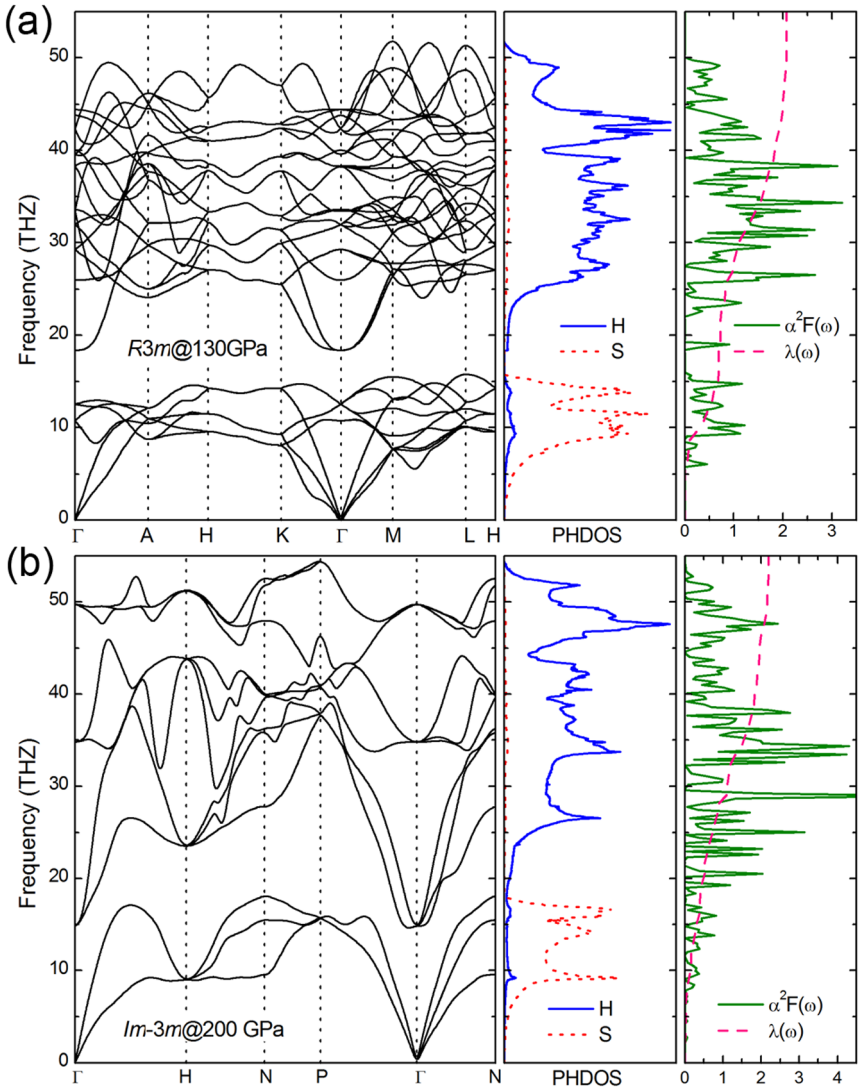

Figure 5 | Phonon properties and Eliashberg spectral function. Phonon dispersion curves, phonon density of states (PHDOS) projected on S and H atoms, and Eliashberg spectral function $\alpha^2F(\omega)$ together with the electron-phonon integral $\lambda(\omega)$ for (a) *R*3*m* at 130 GPa and (b) *Im*-3*m* at 200 GPa.

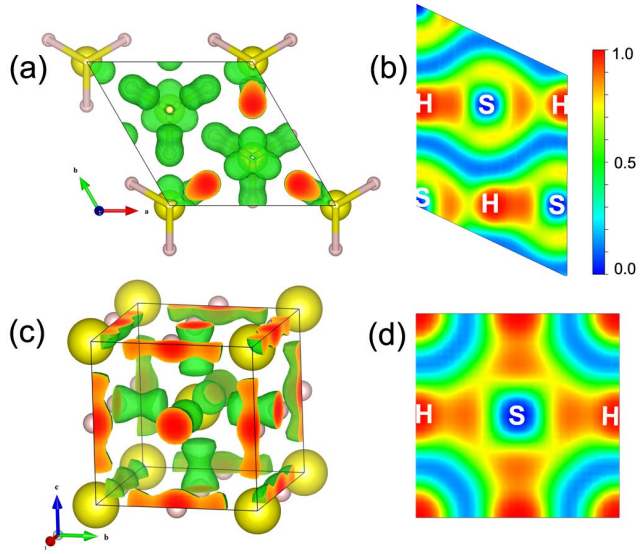

Figure 6 | Calculated ELF of $(H_2S)_2H_2$. The calculated ELF of (a) *R*3*m* with isosurface value of 0.73, (b) *R*3*m* for the (011) plane, (c) *Im*-3*m* with isosurface value of 0.73, (d) *Im*-3*m* for (100) plane.

Notably, the calculated metallization pressure of $(H_2S)_2H_2$ (111 GPa) is within the diamond anvil cell capability. The DFT calculation is well known to underestimate the band gap because of its systematic defects for treating the excited states. Thus, the actual metallization pressure for $(H_2S)_2H_2$ is likely higher than the DFT estimated values in this study. Nevertheless, the calculated metallization pressure for $(H_2S)_2H_2$ is approximately one-third of the suggested pressure for the metallization of solid hydrogen[38]. The estimated maximal T_c of 200 K in $(H_2S)_2H_2$ is higher than those predicted for most hydrogen-containing compounds, such as $SnH_4(H_2)_2$[28], $GeH_4(H_2)_2$[29], and MH_3 (M = Ga, Ge, Si)[17–19]. Our findings represent a significant step toward the understanding of the high pressure behavior of metallic hydrogen and hydrogen-rich hydrides, which can stimulate future high-pressure experiments on structural and conductivity measurements.

Methods

The high-pressure crystal structure of $(H_2S)_2H_2$ were explored by merging the evolutionary algorithm and *ab initio* total-energy calculations, as implemented in the USPEX code[30–32]. Structures (population size: 10–60 structures, increasing with system size) were produced randomly in the first generation. The subsequent generation is created from 60% of the lowest-enthalpy structures of the preceding generation. New structures are created by heredity (60%), permutation (10%), and lattice mutation (30%) operations. The best structure of each generation is also carried over to the next generation. The calculation stops when the best structure does not change for more than 20 generations.

The underlying structure relaxations are performed using density functional theory within the Perdew-Burke-Ernzerhof parameterization of the GGA[43], as implemented in the Vienna *ab initio* simulation package VASP code[44]. The all-electron projector augmented wave method[45] is adopted with the core radii of 0.8 a.u. for H ($1s^2$) and 1.5 a.u. for S ($3s^23p^4$). Brillouin zone (BZ) sampling using a grid of spacing of $2\pi \times 0.05$ Å^{-1} and a plane-wave basis set cutoff of 500 eV are sufficient for the initial search over structures. However, we recalculated the enthalpy curves with higher accuracy using the energy cutoff 800 eV and k-point mesh of $2\pi \times 0.03$ Å^{-1}. These values were selected to ensure that the total energy are well converged to be better than 1 meV/atom.

Lattice dynamics and superconducting properties were calculated using density functional perturbation theory[46] and the plane-wave pseudopotential method with Vanderbilt-type ultrasoft potentials[47], as implemented in the QUANTUM-ESPRESSO code[48]. Convergence tests provide a suitable value of 80 Ry kinetic energy cutoff. The q-point mesh in the first BZ of $3 \times 3 \times 5$ for *R3m* and $8 \times 8 \times 8$ for *Im-3m* structures are used in the interpolation of the force constants for the phonon dispersion curve calculations. A denser k-point mesh $16 \times 16 \times 24$ for *R3m* and $32 \times 32 \times 32$ for *Im-3m* structures are adopted to ensure k-point sampling convergence with a Gaussians width of 0.03 Ry, which approximates the zero width limits in the calculation of EPC parameter λ.

1. Vos, W. L., Finger, L. W., Hemley, R. J. & Mao, H.-K. Novel H_2-H_2O clathrates at high pressures. *Phys. Rev. Lett.* **71**, 3150–3153 (1993).
2. Strobel, T. A., Ganesh, P., Somayazulu, M., Kent, P. R. C. & Hemley, R. J. Novel Cooperative Interactions and Structural Ordering in H_2S-H_2. *Phys. Rev. Lett.* **107**, 255503 (2011).
3. Somayazulu, M. S., Finger, L. W., Hemley, R. J. & Mao, H. K. High-Pressure Compounds in Methane-Hydrogen Mixtures. *Science* **271**, 1400–1402 (1996).
4. Strobel, T. A., Somayazulu, M. & Hemley, R. J. Novel Pressure-Induced Interactions in Silane-Hydrogen. *Phys. Rev. Lett.* **103**, 065701–065704 (2009).
5. Wang, S. B., Mao, H. K., Chen, X. J. & Mao, W. L. High pressure chemistry in the H_2-SiH_4 system. *Proc. Natl. Acad. Sci. USA* **106**, 14763–14767 (2009).
6. Strobel, T. A., Chen, X.-J., Somayazulu, M. & Hemley, R. J. Vibrational dynamics, intermolecular interactions, and compound formation in GeH_4-H_2 under pressure. *J. Chem. Phys.* **133**, 164512–164519 (2010).
7. Lin, Y., Mao, W. L. & Mao, H. Storage of molecular hydrogen in an ammonia borane compound at high pressure. *Proc. Natl. Acad. Sci. USA* **106**, 8113 (2009).
8. Chellappa, R. S., Somayazulu, M., Struzhkin, V. V., Autrey, T. & Hemley, R. J. Pressure-induced complexation of NH_3BH_3-H_2. *J. Chem. Phys.* **131**, 224515–224519 (2009).
9. Loubeyre, P., Letoullec, R. & Pinceaux, J.-P. Compression of $Ar(H_2)_2$ up to 175 GPa: A new path for the dissociation of molecular hydrogen? *Phys. Rev. Lett.* **72**, 1360 (1994).
10. Kleppe, A. K., Amboage, M. & Jephcoat, A. P. New high-pressure van der Waals compound $Kr(H_2)_4$ discovered in the krypton-hydrogen binary system. *Sci. Rep.* **4**, 4989 (2014).
11. Somayazulu, M. *et al.* Pressure-induced bonding and compound formation in xenon–hydrogen solids. *Nat. Chem.* **2**, 50–53 (2010).
12. Mao, W. L. & Mao, H. K. Hydrogen storage in molecular compounds. *Proc. Natl. Acad. Sci. USA* **101**, 708 (2004).
13. Wigner, E. & Huntington, H. B. On the Possibility of a Metallic Modification of Hydrogen. *J. Chem. Phys.* **3**, 764–770 (1935).
14. Ashcroft, N. W. Metallic Hydrogen: A High-Temperature Superconductor? *Phys. Rev. Lett.* **21**, 1748 (1968).
15. Eremets, M. I. & Troyan, I. A. Conductive dense hydrogen. *Nat. Mater.* **10**, 927–931 (2011).
16. Zha, C.-S., Liu, Z. & Hemley, R. J. Synchrotron Infrared Measurements of Dense Hydrogen to 360 GPa. *Phys. Rev. Lett.* **108**, 146402 (2012).
17. Gao, G. *et al.* Metallic and superconducting gallane under high pressure. *Phys. Rev. B* **84**, 064118 (2011).
18. Abe, K. & Ashcroft, N. W. Quantum disproportionation: The high hydrides at elevated pressures. *Phys. Rev. B* **88**, 174110 (2013).
19. Jin, X. *et al.* Superconducting high-pressure phases of disilane. *Proc. Natl. Acad. Sci. USA* **107**, 9969–9973 (2010).
20. Flores-Livas, J. A. *et al.* High-Pressure Structures of Disilane and Their Superconducting Properties. *Phys. Rev. Lett.* **108**, 117004 (2012).
21. Chen, X.-J. *et al.* Pressure-Induced Metallization of Silane. *Proc. Natl. Acad. Sci. USA* **105**, 20–23 (2008).
22. Eremets, M. I., Trojan, I. A., Medvedev, S. A., Tse, J. S. & Yao, Y. Superconductivity in Hydrogen Dominant Materials: Silane. *Science* **319**, 1506–1509 (2008).
23. Chen, X.-J. *et al.* Superconducting Behavior in Compressed Solid SiH_4 with a Layered Structure. *Phys. Rev. Lett.* **101**, 077002 (2008).
24. Martinez-Canales, M. *et al.* Novel Structures and Superconductivity of Silane under Pressure. *Phys. Rev. Lett.* **102**, 087005–087004 (2009).
25. Gao, G. *et al.* Superconducting High Pressure Phase of Germane. *Phys. Rev. Lett.* **101**, 107002–107004 (2008).
26. Zhou, D. *et al.* Ab initio study revealing a layered structure in hydrogen-rich KH_6 under high pressure. *Phys. Rev. B* **86**, 014118 (2012).
27. Wang, H., Tse, J. S., Tanaka, K., Iitaka, T. & Ma, Y. Superconductive sodalite-like clathrate calcium hydride at high pressures. *Proc. Natl. Acad. Sci. USA* **109**, 6463–6466 (2012).
28. Li, Y. *et al.* Superconductivity at 100 K in dense $SiH_4(H_2)_2$ predicted by first principles. *Proc. Natl. Acad. Sci. USA* **107**, 15708–15711 (2010).
29. Zhong, G. *et al.* Structural, Electronic, Dynamical, and Superconducting Properties in Dense $GeH_4(H_2)_2$. *J. Phys. Chem. C* **116**, 5225–5234 (2012).
30. Oganov, A. R. & Glass, C. W. Crystal structure prediction using ab initio evolutionary techniques: Principles and applications. *J. Chem. Phys.* **124**, 244704–244715 (2006).
31. Oganov, A. R., Lyakhov, A. O. & Valle, M. How Evolutionary Crystal Structure Prediction Works—and Why. *Acc. Chem. Res.* **44**, 227–237 (2011).
32. Lyakhov, A. O., Oganov, A. R., Stokes, H. T. & Zhu, Q. New developments in evolutionary structure prediction algorithm USPEX. *Comput. Phys. Commun.* **184**, 1172–1182 (2013).
33. Pickard, C. J. & Needs, R. J. Structure of phase III of solid hydrogen. *Nat. Phys.* **3**, 473–476 (2007).
34. Degtyareva, O. *et al.* Novel chain structures in group VI elements. *Nat. Mater.* **4**, 152–155 (2005).
35. Luo, H., Greene, R. G. & Ruoff, A. L. β-Po phase of sulfur at 162 GPa: X-ray diffraction study to 212 GPa. *Phys. Rev. Lett.* **71**, 2943–2946 (1993).
36. Li, Y., Hao, J., Liu, H., Li, Y. & Ma, Y. The metallization and superconductivity of dense hydrogen sulfide. *J. Chem. Phys.* **140**, 174712 (2014).
37. Simon, A. Superconductivity and Chemistry. *Angew. Chem., Int. Ed.* **36**, 1788–1806 (1997).
38. Azadi, S. & Foulkes, W. M. C. Fate of density functional theory in the study of high-pressure solid hydrogen. *Phys. Rev. B* **88**, 014115 (2013).
39. Allen, P. B. Neutron Spectroscopy of Superconductors. *Phys. Rev. B* **6**, 2577–2579 (1972).
40. Ashcroft, N. W. Hydrogen Dominant Metallic Alloys: High Temperature Superconductors? *Phys. Rev. Lett.* **92**, 187002 (2004).
41. Allen, P. B. & Dynes, R. C. Transition temperature of strong-coupled superconductors reanalyzed. *Phys. Rev. B* **12**, 905–922 (1975).
42. Yao, Y. & Klug, D. D. High-pressure phase transition and metallization in $Ar(H_2)_2$. *Phys. Rev. B* **83**, 020105 (2011).
43. Perdew, J. P., Burke, K. & Ernzerhof, M. Generalized Gradient Approximation Made Simple. *Phys. Rev. Lett.* **77**, 3865–3868 (1996).
44. Kresse, G. & Furthmüller, J. Efficient iterative schemes for ab initio total-energy calculations using a plane-wave basis set. *Phys. Rev. B* **54**, 11169–11186 (1996).
45. Kresse, G. & Joubert, D. From ultrasoft pseudopotentials to the projector augmented-wave method. *Phys. Rev. B* **59**, 1758–1775 (1999).
46. Baroni, S., de Gironcoli, S., Dal Corso, A. & Giannozzi, P. Phonons and related crystal properties from density-functional perturbation theory. *Rev. Mod. Phys.* **73**, 515–562 (2001).
47. Vanderbilt, D. Soft self-consistent pseudopotentials in a generalized eigenvalue formalism. *Phys. Rev. B* **41**, 7892 (1990).
48. Paolo, G. *et al.* QUANTUM ESPRESSO: a modular and open-source software project for quantum simulations of materials. *J. Phys.: Condens. Matter* **21**, 395502 (2009).

Acknowledgments

This work was supported by the National Basic Research Program of China (No. 2011CB808200), Program for Changjiang Scholars and Innovative Research Team in University (No. IRT1132), National Natural Science Foundation of China (Nos. 51032001, 11204100, 11074090, 10979001, 51025206, and 11104102), National Found for Fostering Talents of basic Science (No. J1103202), Specialized Research Fund for the Doctoral Program of Higher Education (20120061120008 and 20110061120007), and China Postdoctoral Science Foundation (2012M511326 and 2013T60314). Parts of calculations were performed in the High Performance Computing Center (HPCC) of Jilin University.

Author contributions

T.C. and D.F.D. designed research. D.F.D. and Y.X.L. performed research. D.F.D., F.B.T., D.L., Z.H.Z., H.Y.Y., X.L.H., B.B.L. and W.J.T. analyzed the data. D.F.D. and T.C. wrote the paper.

Additional information

Supplementary information accompanies this paper at http://www.nature.com/scientificreports

Competing financial interests: The authors declare no competing financial interests.

How to cite this article: Duan, D. *et al.* Pressure-induced metallization of dense $(H_2S)_2H_2$ with high-T_c superconductivity. *Sci. Rep.* **4**, 6968; DOI:10.1038/srep06968 (2014).